chemosensors

MDPI

Article

Fabrication of Palladium-Decorated Zinc Oxide Nanostructures for Non-Enzymatic Glucose Sensing

Reagan Aviha [1], Anju Joshi [1] and Gymama Slaughter [1,2,*]

[1] Center for Bioelectronics, Old Dominion University, Norfolk, VA 23508, USA
[2] Department of Electrical and Computer Engineering, Old Dominion University, Norfolk, VA 23508, USA
* Correspondence: gslaught@odu.edu

Abstract: The growing global burden of diabetes necessitates the development of glucose sensors that are not only reliable and sensitive but also cost-effective and amenable to point-of-care use. In this work, we report a non-enzymatic electrochemical glucose sensor based on laser-induced graphene (LIG), functionalized with zinc oxide (ZnO) and palladium (Pd) nanostructures. The ZnO nanostructures were systematically optimized on the LIG surface by varying electrochemical deposition parameters, including applied potential, temperature, and deposition time, to enhance the electrocatalytic oxidation of glucose in alkaline medium. Subsequent modification with Pd nanostructures further improved the electrocatalytic activity and sensitivity of the sensor. The performance of the LIG/ZnO/Pd sensor was investigated using chronoamperometric and cyclic voltammetric analysis in 0.1 M NaOH at an applied potential of 0.65 V. The sensor exhibited a wide dynamic range (2–10 mM; 10–24 mM) with a limit of detection of 130 µM, capturing hypo- and hyperglycemia conditions. Moreover, a sensitivity of 25.63 $\mu A \cdot mM^{-1} \cdot cm^{-2}$ was observed. Additionally, the sensor showcased selective response towards glucose in the presence of common interferents. These findings highlight the potential of the LIG/ZnO/Pd platform for integration into next-generation, non-enzymatic glucose monitoring systems for clinical and point-of-care applications.

Keywords: non-enzymatic; glucose; sensor; zinc oxide; palladium; nanostructures

check for updates

Received: 27 April 2025
Revised: 20 May 2025
Accepted: 30 May 2025
Published: 1 June 2025

Citation: Aviha, R.; Joshi, A.; Slaughter, G. Fabrication of Palladium-Decorated Zinc Oxide Nanostructures for Non-Enzymatic Glucose Sensing. *Chemosensors* **2025**, *13*, 201. https://doi.org/10.3390/chemosensors13060201

Copyright: © 2025 by the authors. Licensee MDPI, Basel, Switzerland. This article is an open access article distributed under the terms and conditions of the Creative Commons Attribution (CC BY) license (https://creativecommons.org/licenses/by/4.0/).

1. Introduction

Diabetes mellitus is considered a chronic metabolic disorder that has emerged as a critical global health concern due to its increasing prevalence and severe complications. The most common and debilitating consequences remain diabetic neuropathy and the accumulation of advanced glycation end products, which can trigger kidney inflammation, leading to multi-organ failure [1,2]. In the United States alone, diabetes affects approximately 38 million individuals (11.6% of the population), with an estimated 8.7 million remaining undiagnosed [3]. Additionally, diabetes also imposes a profound economic burden, with annual healthcare costs reaching USD 412.9 billion in 2022, with an average per-person cost of USD 19,736, which is 2.6 times higher than for individuals without diabetes [4,5]. On a global scale, the number of diabetes cases has increased by 338% over the past 17 years, and current projections estimate this figure will reach 853 million by 2050 [6].

Blood glucose ($C_6H_{12}O_6$) is considered a crucial component associated with metabolic processes like glycolysis and glycogenesis. The normal glucose levels lie between 4.4 and 5.0 mM and are maintained due to insulin. However, levels exceeding 11 mM indicate hyperglycemia, while those below 2.8 mM can trigger hypoglycemic seizures [7,8]. The

concentration-dependent relevance necessitates that patients and clinicians manage glucose levels effectively [9]. The existing diagnostics for glucose monitoring include optical, electrochemical, acoustic, and electromagnetic sensors. However, the existing diagnostics face challenges like signal interference, photobleaching, and sensitivity issues [10,11]. Electrochemical sensors are considering promising attributed to their specificity, sensitivity, affordability, and ease of integration [12,13]. These electrochemical sensors can be conveniently categorized into enzymatic and non-enzymatic types. Enzymatic electrochemical sensors have progressed through the development of three generations, focusing on sensitivity and lowering operational voltage, but suffer due to enzyme instability and mediator toxicity [14–17]. As a suitable alternative, non-enzymatic sensors are often considered as fourth generation, exploring the use of the exceptional electrocatalytic capabilities of the nanostructured catalysts with improved durability and convenience. The approach involves the direct electrocatalytic oxidation of glucose on nanostructured electrode surfaces in alkaline media [18].

Therefore, different nanostructured materials like noble metals (Au [19], Ag [20], Pd [21] and Pt [22]), transition metals (Cu [23], Ni [24], Co [25], and Fe [26]), metal oxides (ZnO [27–29], Fe_2O_3 [30], Co_3O_4 [31] and CuO [32]), alloys (Pd-Mn [33], Cu-Ni [34], Cu3Al [35], Ag-Au [36] and NiFe [37]), carbonaceous nanostructures [38–40], and polymers [41,42]) have been explored towards the enzyme-less electrochemical sensing of glucose with good sensitivity, stability, and catalytic efficiency. In this regard, zinc oxide (ZnO) nanostructures have been widely explored due to their biocompatibility, high surface area, and catalytic activity for glucose sensing [43]. Jia et al. employed an innovative green synthesis approach to modify nitrogen-doped carbon with nano-ZnO to attain a sensitivity of 255 $\mu A \cdot mM^{-1} \cdot cm^{-2}$ over a detection range of 2 μM to 3.28 mM with a limit of detection (LOD) of 0.39 μM [44]. There have been numerous reports focused on enhancing the potential of ZnO nanostructures through doping with other transition-metal nanostructures to attain a significant electrochemical response towards glucose. For instance, Mahmoud et al. developed a Cu-doped ZnO sensor for an ultra-sensitive low limit detection of glucose over a linear range (1 nM to 100 μM) with an LOD of 0.7 nM [45]. Further, composites of Cu_xO-ZnO nanostructures were explored towards attaining a wider detection range (0.03–3.0 mM) with a sensitivity of 384 $\mu A mM^{-1} cm^{-2}$ [46]. A similar response was obtained by Cheng et al., who developed CuO-decorated ZnO structures for a higher glucose range (5–25 mM) in the detection of glucose [47]. Therefore, it is of utmost importance to modify ZnO nanostructures with electrocatalytic nanostructures to offer a wide detection range and low LOD. In this regard, noble metal (e.g., palladium (Pd) [48], platinum (Pt) [49], and silver (Ag) [50]) nanostructures have shown promising applications for the modification of ZnO nanostructures for non-enzymatic glucose sensing.

Among all, Pd has attracted significant attention for non-enzymatic glucose sensing due to its excellent electrocatalytic activity in alkaline media, coupled with a lower overpotential for glucose oxidation compared to Pt and Au [51]. In addition to its favorable catalytic properties, Pd readily forms stable composites with various transition metal oxides [52]. These advantages make Pd a highly promising material for the development of efficient and affordable glucose sensors, particularly in hybrid configurations aimed at enhancing surface reactivity and electron transfer kinetics [53]. However, these reports are scantily available in the literature. In this direction, Yang et al. reported a hydrothermally modified composite of palladium nanostructures with zinc oxide on carbon cloth [48]. The developed sensor enabled a LOD of 0.52 μM over a wide detection range (0.1 μM–10 mM) of glucose. Likewise, Pt nanoparticle-modified ZnO nanorods were synthesized through physical adsorption on a glass substrate for the enzyme-less sensing of glucose [49]. The sensor demonstrated a comparable electrochemical response with

a detection range of 0 to 8 mM and a sensitivity of 32.05 $\mu A \cdot mM^{-1} \cdot cm^{-2}$. Additionally, Lin et al. [50] fabricated Ag-decorated vertically aligned ZnO nanorods on a silicon wafer to attain an exceptional sensitivity of 2792 $\mu A \cdot mM^{-1} \cdot cm^{-2}$ towards glucose. However, the detection range (50–175 μM) for the fabricated sensor was significantly lower to deal with hyperglycemic conditions in a point-of-care setting. Although Wu et al. reported a promising non-enzymatic electrochemical glucose sensor based on a synergistic combination of graphene, Pd, and ZnO on nickel (Ni) foam [27], several limitations remain that constrain its clinical utility. Despite achieving an ultra-low detection limit of 0.056 μM and high sensitivities of 129.44 and 213.3 μA mM^{-1} cm^{-2}, the sensor's linear detection range (5 μM to 6 mM) falls short of addressing glucose concentrations typically encountered in hyperglycemic patients, where physiological levels can exceed 7 mM. This discrepancy diminishes its diagnostic significance for diabetic monitoring and undermines its potential for real-world applications, particularly for continuous glucose monitoring (CGM) in hyperglycemic states.

Recently, there have been extensive efforts towards the development of cost-effective, flexible laser-induced graphene (LIG)-based sensors for diverse clinically relevant biomolecules [54–56]. LIG offers exceptional electrical conductivity and serves as a porous, conductive 3D framework for anchoring functional nanomaterials [57,58]. Here, this work highlights the uniform growth of ZnO nanostructures onto the porous LIG framework to enhance surface reactivity and provide multiple sites for Pd nanostructures to nucleate and further grow to ensure a sensitive electrocatalytic oxidation of glucose. We systematically investigated the growth of ZnO at the axes of applied potential, temperature, time, and precursor concentration to ensure a well-distributed, high-surface-area nanostructured interface which is synergistically combined with optimized Pd nanostructures for a sensitive and selective electrocatalytic oxidation of glucose. The fabricated LIG/ZnO/Pd sensor demonstrated a wide dynamic linear range (low detection range: 2–10 mM; high detection range: 10–24 mM) covering hypoglycemia and hyperglycemia ranges, with a LOD of 130 μM. The sensor also demonstrated excellent sensitivity (25.63 $\mu A \cdot mM^{-1} \cdot cm^{-2}$) and stability towards glucose detection. Moreover, the sensor was able to selectively detect glucose in the presence of interfering species such as maltose, sucrose, fructose, ascorbic acid, uric acid, and dopamine. Therefore, in this study, we introduce a facile, scalable, two-step electrochemical deposition strategy for modifying LIG with ZnO/Pd nanostructures to create a high-performance, enzyme-free glucose sensor.

2. Experimental Section

2.1. Chemicals and Materials

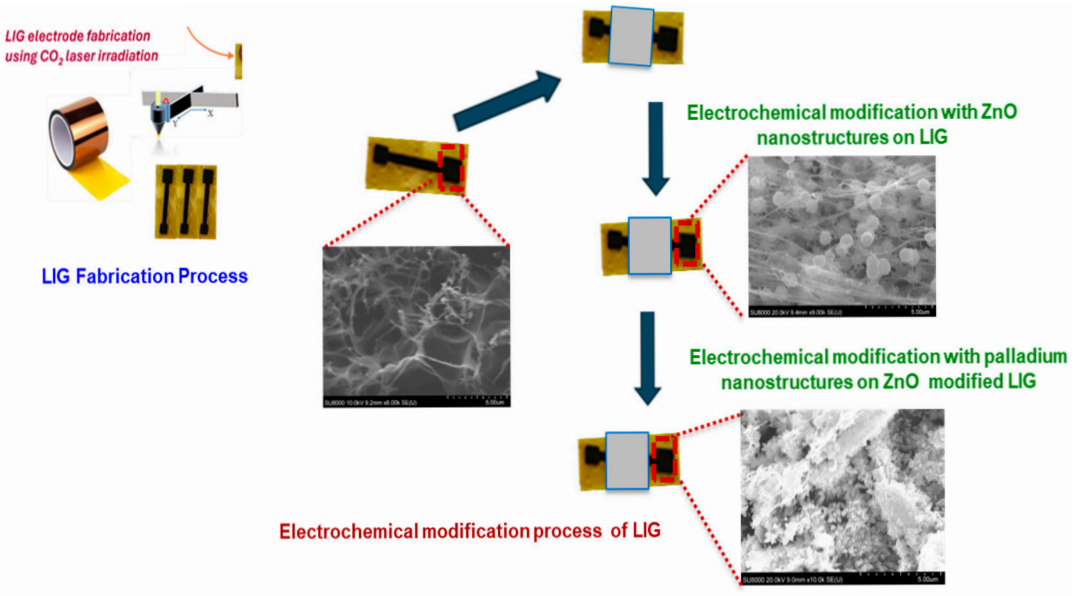
Zinc nitrate hexahydrate ($Zn(NO_3)_2 \cdot 6H_2O$, 98%), potassium chloride (KCl, 99%), palladium chloride ($PdCl_2$, 99%), D-(+) maltose ($C_{12}H_{22}O_{11}.H_2O$, ≥ 99.0%), D-(+) glucose ($C_6H_{12}O_6$, ≥ 99%), uric acid ($C_5H_4N_4O_3$, ≥ 99.0%), potassium ferricyanide ($K_3[Fe(CN)_6]$, 99%), potassium phosphate monobasic (KH_2PO_4, 99%), sodium dibasic phosphate (Na_2HPO_4, ≥ 99.0%), ethanol (94–96%), and acetic acid (CH_3COOH, 99.7%) were obtained from Sigma-Aldrich. D-(−) fructose ($C_6H_{12}O_6$, ≥ 99%) was obtained from ACROS. Sucrose ($C_{12}H_{22}O_{11}$, ≥ 99.0%) was obtained from Thermos Scientific. L-(+) ascorbic acid ($C_6H_8O_6$, 99.0 + %) and dopamine ($C_8H_{11}NO_2$, 99.0%) were obtained from Alfa Aesar. Sodium acetate ($C_2H_3NaO_2$, ≥ 99.0%), sodium hydroxide (NaOH), and sodium chloride (NaCl) were obtained from Fisher Chemical Scientific. The aqueous solutions were prepared with ultrapure deionized (DI) water with a conductivity of 18.20 MΩ. Kapton polyimide (PI) tape procured from TapeMaster (Troy, MI, USA) and polyethylene terephthalate (PET) sheets were used as the base for LIG fabrication.

2.2. Apparatus

The electrochemical performance of the fabricated Pd/ZnO-modified LIG-based sensor was characterized using a Metrohm Dropsens (μStat-i-MultiX) electrochemical workstation. The set-up involves LIG as the working electrode (WE), platinum wire (Pt) electrode as the counter electrode (CE), and an Ag/AgCl/3 M NaCl electrode as the reference electrode. A two-step modification process involving chronoamperometric technique was used for the uniform modification of the LIG with ZnO nanostructures followed by Pd nanostructures. The electrochemical characterization of the Pd/ZnO/LIG nanostructured electrodes was evaluated towards non-enzymatic glucose detection using a chronoamperometric technique at a fixed potential of +0.65V. A morphological and compositional analysis of the electrochemically synthesized Pd/ZnO composites on the LIG surface was conducted using a field emission scanning electron microscope (FE-SEM, JSM-IT700HR InTouchScope™, JEOL USA, Inc., Peabody, MA). Elemental analysis was performed using energy-dispersive X-ray spectroscopy (EDXS) integrated with the SEM.

2.3. Fabrication of the LIG Electrodes

LIG electrodes were fabricated by first designing a 4 mm × 4 mm active surface area using the in-built LightBurn software (v. 0.909). A 1.25 cm-wide strip of polyimide (PI) tape was placed on a flexible PET substrate to ensure mechanical support. The PI layer was then patterned using a CO_2 pulsed laser system (BOSS LS1416, Sanford, FL, USA), operated through LightBurn software. The laser parameters were optimized at a speed of 250 mm/s, 20% maximum power, and a focal height of 20 mm. After laser processing, nail enamel was applied to define the electroactive area and contact pads, effectively isolating the functional regions of the electrode. The electrodes were thoroughly rinsed with deionized water to remove any residual debris. Finally, a ZnO/Pd nanocomposite was electrodeposited onto the LIG surface to enable the non-enzymatic sensing of glucose as illustrated in Scheme 1.



Scheme 1. A schematic representation of the electrochemical modification of laser-induced graphene (LIG) electrode with zinc oxide (ZnO) and palladium (Pd) electrodeposited nanostructures.

3. Results and Discussions

3.1. Optimization of ZnO/Pd Modified LIG Electrodes

The intrinsic electrocatalytic activity of the LIG electrodes were investigated using cyclic voltammetry under variable glucose concentrations (Figure S1, Supporting Infor-

mation). The electrochemical response of the bare LIG was found to exhibit insignificant electroactivity towards glucose, necessitating further modification with nanostructured catalysts capable of catalyzing glucose oxidation. Therefore, ZnO nanostructures were grown and optimized at the axes of potential, temperature, duration, and Zn precursor concentration to ensure a significant electrocatalytic response towards glucose.

An initial seed layer of ZnO was grown on the LIG surface by performing ten sequential cyclic voltammetric scans within a potential range of 0.0 to −1.4 V in 10 mM $Zn(NO_3)_2{\cdot}6H_2O$ solution containing 0.1 M KCl at a temperature of 70 °C. The growth of ZnO nanostructures on LIG was modulated at variable deposition potentials (−0.85 V, −1.0 V, −1.15 V, and −1.25 V) using a chronoamperometric technique in 10 mM $Zn(NO_3)_2{\cdot}6H_2O$ solution at 70 °C under stirring conditions (125 rpm). The choice of deposition potential values was considered based on the preliminary cyclic voltammograms obtained at an unmodified LIG in 10 mM of zinc nitrate solution containing 0.1 M KCl (Figure S2, Supporting Information). The resulting LIG/ZnO electrodes grown at the various potentials were evaluated for electrocatalytic oxidation of glucose, as shown in Figure 1a. Figure S3a (Supporting Information) provides the corresponding concentration-dependent chronoamperometric response for the different potential variants. Additionally, at lower potential values (−0.85 V and −1.0 V), the deposition process of ZnO resulted in a sparse distribution of nanostructures, whereas increasing the potential values to −1.15 V led to the formation of dense ZnO nanostructures [59]. At higher potential values (−1.25 V), the ZnO nanostructures agglomerated due to the accelerated deposition process [60]. Although there was no significant variability in the electrochemical response for the different potential variants, the performance of LIG/ZnO nanostructures grown at a potential of −1.15 V exhibited a slightly higher sensitivity compared to the other potential variants and was selected for further investigation. The growth of the ZnO nanostructures on LIG was monitored under variable temperatures ranging from 35 °C to 90 °C at a constant deposition potential of −1.15 V. The resulting LIG/ZnO nanostructures were evaluated for the electrocatalytic oxidation of glucose depicted in Figure 1b (Figure S3b, Supporting Information).

A significantly higher sensitivity was observed for the ZnO nanostructures grown at a temperature of 50 °C and therefore was further explored for the Zn precursor optimization. Here, the electrochemical deposition of ZnO follows a temperature-dependent reaction pathway involving the reduction in nitrate and dissolved oxygen, leading to hydroxide ion generation and the subsequent formation of zinc hydroxide and ZnO [61]:

$$NO_3^- + H_2O + 2e^- \rightarrow NO_2^- + 2OH^- \ldots \text{(precursor breaking down)}$$

$$O_2 + 2H_2O + 4e^- \rightarrow 4OH^- \ldots \text{(oxygen dissolution)}$$

$$Z_n^{2+} + 2OH^- \rightarrow Z_n(OH)_2 \ldots \text{(zinc hydroxide formation)}$$

$$Z_n(OH)_2 \rightarrow Z_nO + H_2O \ldots \text{(ZnO formation)}$$

Although the crystalline structure of ZnO is more favorable at higher temperatures (over 70 °C), the deposition at 50 °C likely results in a mixed-phase composition of ZnO and $Zn(OH)_2$. The presence of $Zn(OH)_2$ is advantageous for glucose sensing, as its abundant surface hydroxyl groups promote enhanced glucose adsorption and facilitate electrocatalytic oxidation. Following oxidation, the Zn–OH catalytic sites are regenerated via interaction with OH^- ions in the electrolyte, thus sustaining the redox catalytic cycle. At a constant potential (−1.15 V) and temperature (50 °C), the impact of growth duration (5, 10, 20, and 30 min) on the electrochemical performance towards glucose was investigated. As shown in Figure 1c, the ZnO nanostructures grown on LIG at the 5 and 10 min exhibited low electrocatalytic capability toward glucose and this may be attributed to the sparsely

distributed nanostructures on LIG electrode. Increasing the duration to 20 min resulted in a LIG/ZnO nanostructured electrode with significant electrochemical response towards glucose. Further increasing the growth duration to 30 min resulted in agglomerate ZnO layers and lower electrocatalytic activity towards glucose. The decline in electrocatalytic activity observed for ZnO nanostructures grown on LIG for 30 min can be attributed to the agglomeration of the nanostructures. It is expected that extended growth duration leads to an increase in ZnO crystallite size with a decrease in defect density, which may reduce the availability of catalytically active sites for the electrocatalytic oxidation of glucose. Additionally, agglomerated ZnO nanostructures tend to limit the overall electrochemically active surface area and hinder the effective diffusion of glucose molecules to the inner catalytic sites, leading to a reduction in electrocatalytic activity under prolonged durations. These observations support the optimal growth condition of ZnO nanostructures on LIG electrodes at −1.15V and 50 °C for 20 min (Figure S3c, Supporting Information). In addition, the impact of Zn precursor ($Zn(NO_3)_2 \cdot 6H_2O$) concentrations (5, 10, 20, and 25 mM) on the growth of ZnO nanostructures on the LIG electrode and the corresponding electrochemical performance towards glucose were also investigated. Based on the comparative electrochemical response depicted in Figure 1d (Figure S3d, Supporting Information), 20 mM $Zn(NO_3)_2 \cdot 6H_2O$ was chosen to be the optimum concentration for the growth of ZnO nanostructures on LIG. Therefore, subsequent ZnO nanostructures on LIG were synthesized at a potential of (−1.15 V), temperature (50 °C), duration (20 min), and precursor concentration ($Zn\ (NO_3)_2 \cdot 6H_2O$) (20 mM).

The successful optimization of the ZnO nanostructures on the LIG electrode was further followed by the electrochemical deposition of palladium (Pd) nanostructures in a 2 mM $PdCl_2$ solution prepared in 0.1 M acetic buffer. Pd is widely recognized for its exceptional electrocatalytic activity for glucose oxidation in alkaline media, attributed to its favorable d-band electronic structure, which enhances the adsorption and dehydrogenation of glucose molecules [62]. The growth of the Pd nanostructures on ZnO nanostructured LIG was optimized under variable deposition potentials (+0.10, −0.05, −0.20, −0.35, and −0.50 V) and were investigated in 5 mM potassium ferrocyanide in 0.1 M KCl (redox probe). The deposition potentials for the Pd growth were chosen based on the cyclic voltametric studies carried out in 2 mM $PdCl_2$ solution in acetic acid (Figure S4, Supporting Information). As seen in Figure 2a, Pd nanostructures deposited at a potential of (−0.20V) demonstrated a significantly enhanced electrochemical response than other potential variants, suggesting an enhanced electron transfer kinetics. The electrodeposition of Pd nanostructures was found to be more effective at negative potentials (−0.05, −0.2, −0.35, and −0.50 V) compared to a positive potential (0.10 V), which aligns with previous literature [63]. A potential of −0.2 V facilitates the accelerated nucleation and growth of Pd, forming high-surface-area hierarchical nanostructures that enhance electron transfer kinetics. However, further increasing the negative potential results in non-uniform Pd growth accompanied by surface cracks and hydrogen evolution. These effects cause an uneven modification of the sensor surface, ultimately leading to decreased electron transfer efficiency as in other literature [63]. Moreover, the impact of different growth durations (1.5 min, 2.5 min, 3.5 min, and 4.5 min) was evaluated. As shown in Figure 2b, Pd nanostructures grown for 2.5 min yielded enhanced electron transfer kinetics attributed to a uniform well-oriented Pd nanostructure on the LIG/ZnO electrode. The synergistic combination of resulting LIG/ZnO/Pd electrodes was explored for the electrochemical characterization of glucose.

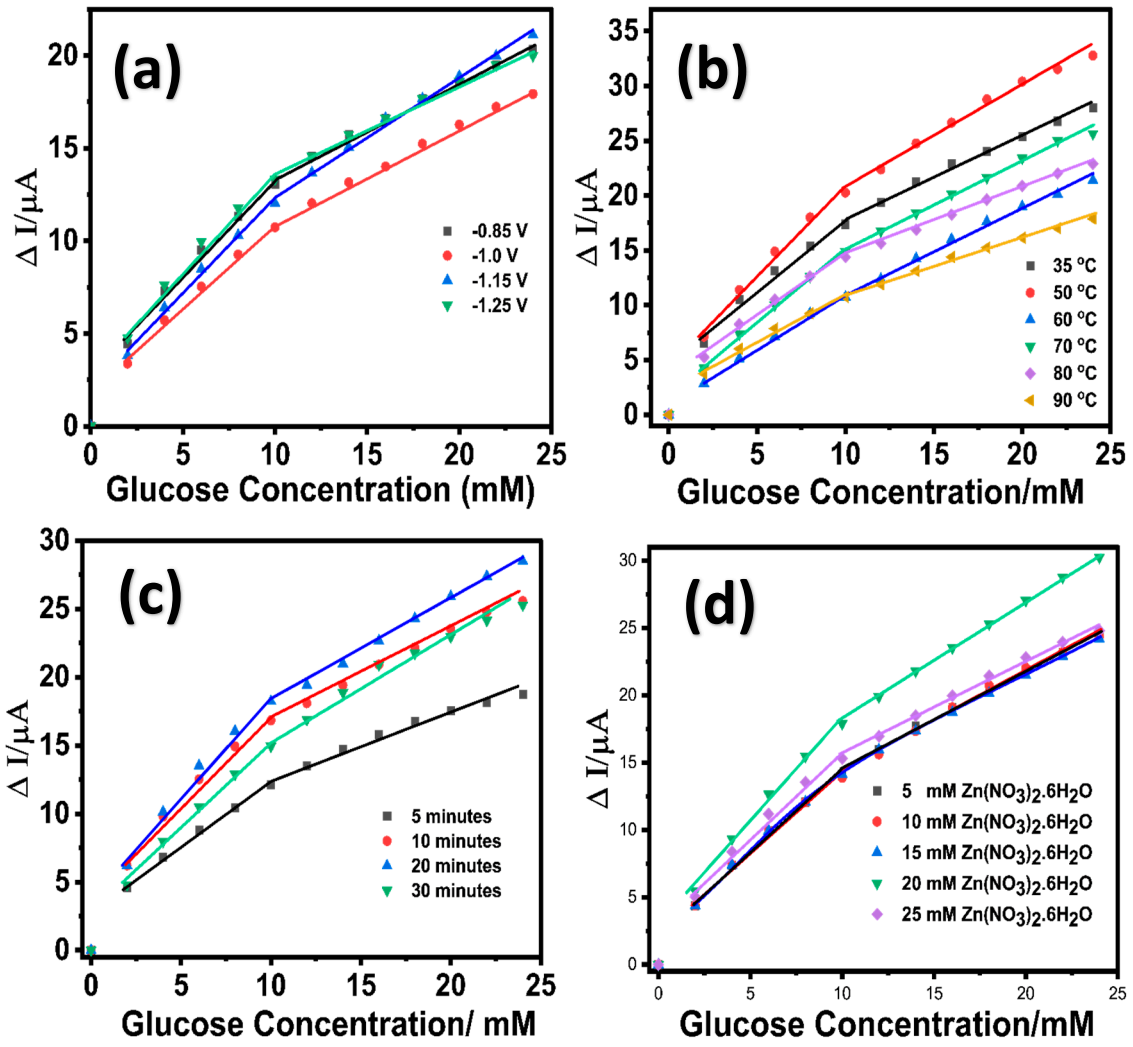


Figure 1. Linear calibration response of LIG/ZnO electrode towards glucose oxidation in 0.1 M NaOH at variable (**a**) potentials; (**b**) temperature; (**c**) time; (**d**) $Zn(NO_3)_2.6H_2O$ concentration.

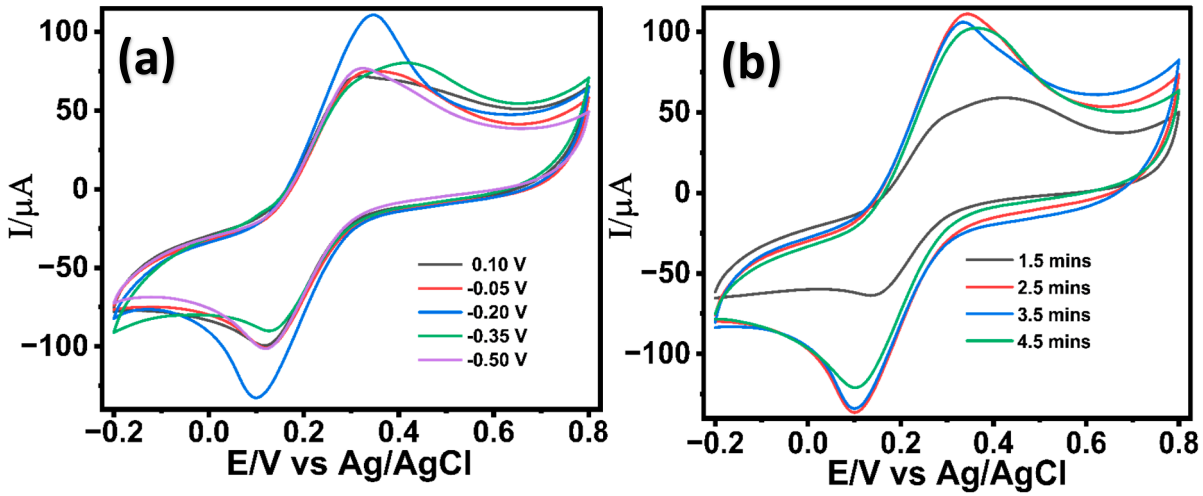


Figure 2. Cyclic voltametric response of LIG/ZnO/Pd electrodes in 5 mM $K_3[Fe(CN)_6]^{3-}$ in 0.1 M KCl at variable (**a**) potentials and (**b**) durations.

3.2. Physical Characterization of LIG-Modified Electrodes

The morphology of the LIG electrodes was investigated using the scanning electron microscopic technique. As seen in Figure 3a, the LIG surface displayed a highly fibrous and porous 3D interconnected morphology. The porous network observed in the LIG electrodes is attributed to the laser-induced ablation process which breaks bonds such as C–O, C=O, and N–C, creating a high-density defect structure [64]. Figure 3b shows the presence of spherical ZnO nanostructures uniformly grown on the LIG electrode. The electrodeposition of Pd nanostructures was performed in a mildly acidic medium (pH ≈ 5.0), which resulted in the formation of surface ridges on the ZnO nanostructures. These morphological changes are not detrimental; rather, they enhance the surface area without compromising the structural or electrochemical integrity of the LIG/ZnO substrate, suggesting successful modification of the LIG electrode (Figure 3c). Energy-dispersive X-ray (EDAX) analysis revealed the presence of C, O, Zn, and Pd with atomic percentages of 47.84%, 24.33%, 26.55%, and 0.09%, respectively, for the Pd/ZnO/LIG electrodes (Figure S5, Supporting Information).

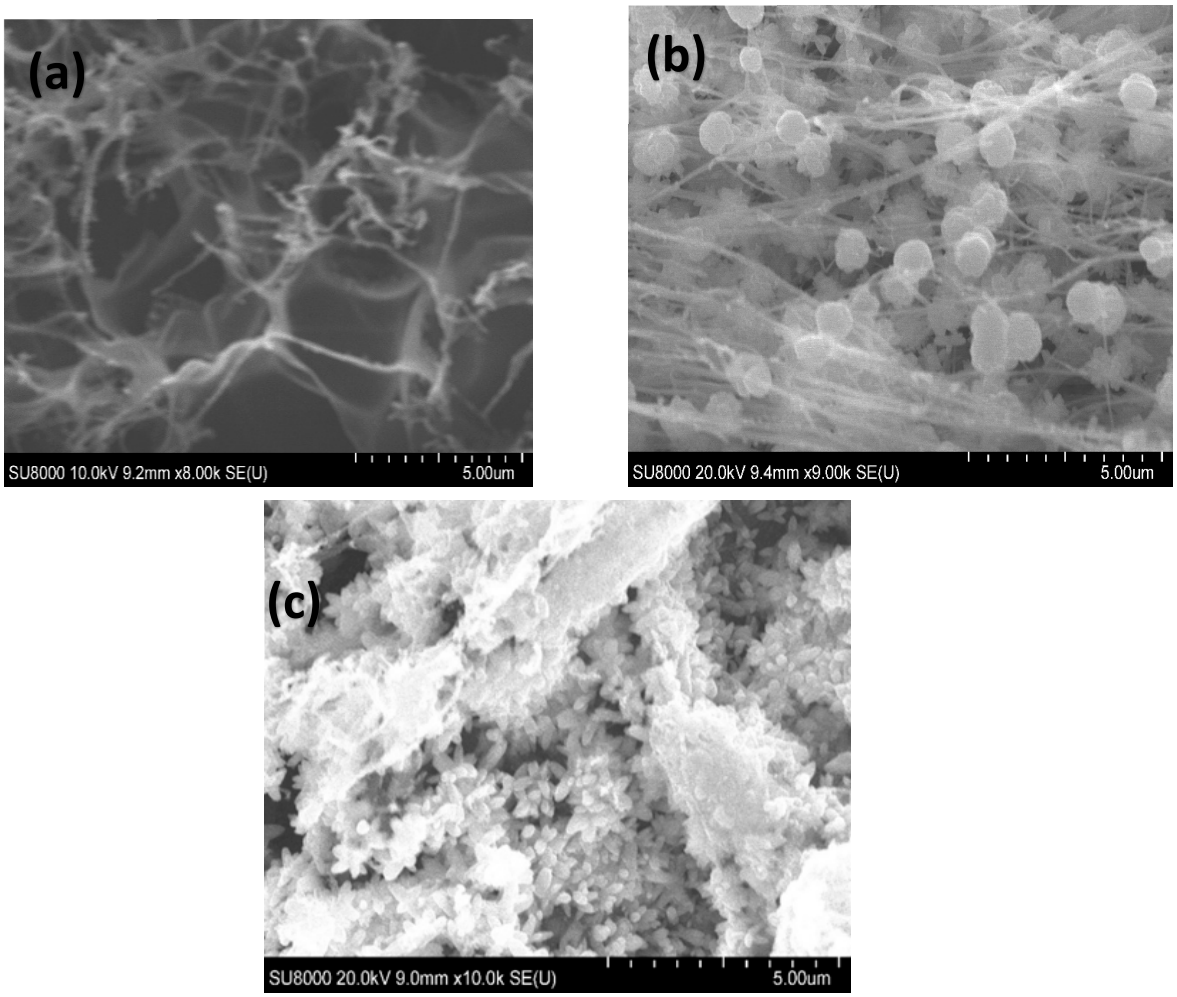


Figure 3. Scanning electron micrograph of the fabricated (**a**) LIG, (**b**) LIG/ZnO, (**c**) LIG/ZnO/Pd electrodes.

3.3. Electrochemical Characterization of LIG/ZnO/Pd Electrodes

The electron transfer kinetics of the fabricated electrodes were systematically investigated using cyclic voltammetry in a 5 mM potassium ferricyanide ($K_3[Fe(CN)_6]$) solution containing 0.1 M KCl. The bare LIG electrode exhibited two well-defined redox peaks

corresponding to the reversible redox reaction of $[Fe(CN)6]^{4-}$/$[Fe(CN)6]^{3-}$, demonstrating the intrinsic electron transfer capability of the LIG substrate (Figure 4a). Upon modification with ZnO nanostructures, an enhancement in the electrochemical response was observed and attributed to the high surface area and favorable electron transport properties introduced by the semiconducting ZnO nanostructures. The LIG/ZnO/Pd nanostructured electrode resulted in a significant increase in redox current, indicating a significant improvement in electron transfer kinetics. The observed electrochemical response is attributed to the synergistic electrocatalytic capabilities of Pd, ZnO, and conductive LIG, which creates an efficient electron-conducting pathway and active sites for redox activity [65], thereby facilitating fast electron transfer kinetics. Additionally, the 3-dimensional porous network of LIG provided anchoring sites for the growth of ZnO and Pd nanostructures and facilitated mass transfer leading to an enhanced electron mobility within the composite sensor material [66]. To assess the individual contributions of ZnO and Pd, binary composites (LIG/ZnO and LIG/Pd) were also evaluated. Both showed improved electrochemical responses relative to bare LIG attributed to the ZnO's high surface area and semiconducting nature, and Pd's inherent catalytic activity. However, their performance remained notably lower than the ternary LIG/ZnO/Pd system. These results confirm that the integrated ternary architecture offers a pronounced synergistic effect, enhancing redox activity than either binary combination alone.

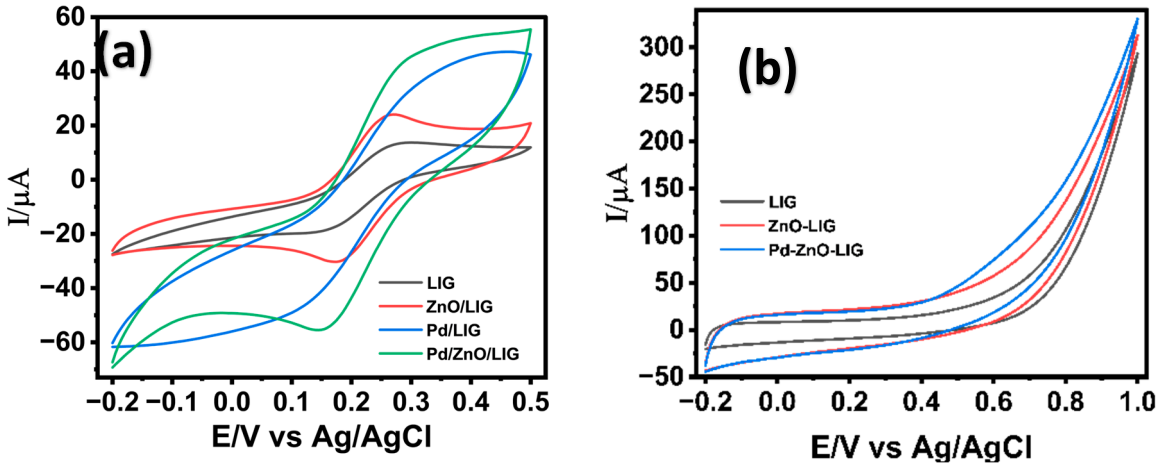


Figure 4. Cyclic voltammogram of LIG-modified electrode surfaces in the presence of (**a**) 5.0 mM $K_3[Fe(CN)_6]$ in 0.1 M KCl; (**b**) 2 mM glucose in 0.1 M NaOH. Scan rate of 50 mV/s.

The LIG/ZnO/Pd-based sensor's electrocatalytic performance towards glucose oxidation in 0.1 M NaOH was examined. Cyclic voltammetry was carried out in 0.1 M NaOH containing 2 mM glucose at variable modified LIG surfaces, as shown in Figure 4b. The bare LIG electrode showed a negligible anodic response, indicating poor catalytic activity toward glucose oxidation. Modification with ZnO nanostructures showed a modest increase in anodic current, which is attributed to the enhanced surface area and partial facilitation of electron transfer through ZnO nanostructures on the LIG sensor's surface. The uniform modification of the LIG electrodes with Pd nanostructures resulted in a sharp and well-defined anodic increase in current at an onset potential of ca. 0.6 V, signifying a substantial improvement in electrocatalytic activity towards the oxidation of glucose. This enhanced response is attributed to the high electrocatalytic efficiency of Pd towards glucose oxidation, as well as the synergistic activity of Pd, ZnO, and LIG. The composite nanostructured electrode provides an integrated platform with redox active sites, excellent conductivity, and efficient charge transfer kinetics, making it a promising candidate for non-enzymatic glucose detection.

3.4. Electrocatalytic Performance of LIG/ZnO/Pd-Based Glucose Sensor

The electrochemical response of the LIG/ZnO/Pd sensor toward the electrocatalytic oxidation of glucose was investigated using cyclic voltammetry (Figure S5, Supplementary Information) and chronoamperometry (Figure 5) techniques in 0.1 M NaOH. The cyclic voltametric analysis was performed in the presence of varying concentrations of glucose within a potential range of –0.2 V to +1.0 V at a scan rate of 50 mV/s. As shown in Figure S6 (Supplementary Information), in the presence of 0.1 M NaOH, insignificant electrocatalytic activity was observed. Upon the addition of glucose, an electrocatalytic activity towards glucose was observed at the onset potential of ca. +0.60 V, suggesting the electrocatalytic oxidation of glucose following the reaction mechanisms below [49]:

$$Pd + 2OH^- \rightarrow \mathrm{Pd}(OH)_2 + 2\mathrm{e}^- \quad (1)$$

$$Pd(OH)_2 + OH^- \rightarrow PdOOH + H_2O + \mathrm{e}^- \quad (2)$$

$$PdO(H)_2 + C_6H_{12}O_6 \rightarrow P_d(OH)_2 + C_6H_{12}O_7 \quad (3)$$

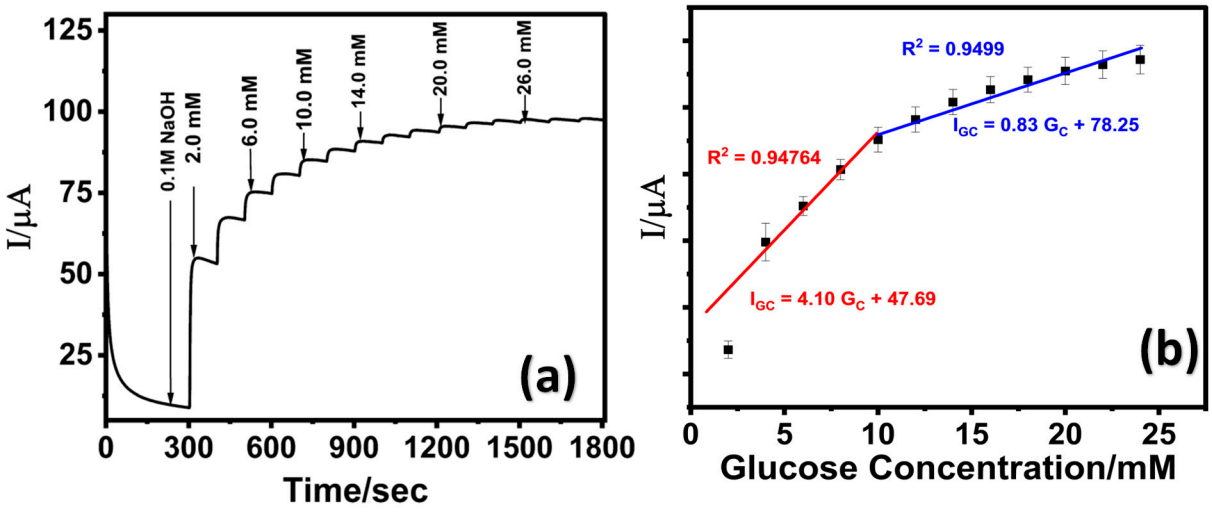


Figure 5. (**a**) Chronoamperometric response of LIG/ZnO/Pd at varying glucose concentration in 0.1 M NaOH; (**b**) corresponding calibration curve.

With increasing glucose concentrations, a positive shift in the oxidation onset potential was observed, which is attributed to the increased adsorption of glucose or intermediates on the electrode's catalytic active sites, thereby altering the surface reaction kinetics. The electrocatalytic oxidation of glucose on the LIG/ZnO/Pd sensor surface is governed by a Langmuir-type adsorption–desorption mechanism. In this process, glucose molecules initially adsorb onto the active sites of the sensor, where they undergo oxidation to gluconolactone. At higher glucose concentrations, the accumulation of oxidation products may lead to partial blockage of these active sites. Additionally, this buildup can alter the local diffusion gradient, hindering the effective transport of glucose molecules to the electrode surface. These effects contribute to a shift in the oxidation potential, resulting in an increased overpotential during the sensing process [67,68].

The chronoamperometric analysis was performed at a fixed potential of 0.65 V. A stepwise increase in oxidative current with subsequent increase in glucose concentrations (2 mM each) was observed as shown in Figure 5a. The corresponding calibration curve (Figure 5b) exhibited extended linear range (low detection range: 2–10 mM; high detection range: 10–24 mM) suggesting a transition in the electrocatalytic oxidation mechanism of glucose, from an adsorption-controlled process at lower concentrations to a diffusion--limited

process at higher concentrations. As illustrated in Figure 5b, at low glucose concentrations, the molecules adsorb onto the LIG/ZnO/Pd sensor surface and are efficiently oxidized due to the availability of multiple active sites, resulting in a linear increase in peak current. However, at higher glucose concentration, the active sites become progressively saturated, and the system transitions to a diffusion-limited regime, where mass transport becomes the rate-determining step, leading to a reduced sensitivity as reported in other studies [69,70].

The calculated limit of detection (LOD) of 130 µM was attained using 3σ/S [71], where σ represents the standard deviation of the blank signal (n = 3) and S represents the slope of the calibration curve. The sensitivity was calculated to be 25.63 $\mu A \cdot mM^{-1} \cdot cm^{-2}$. Moreover, the electrochemical performance of the fabricated LIG/ZnO/Pd sensor was found to be comparable with existing literature and exhibited an extended dynamic linear range with a fabrication time of 28 min. A detailed comparative analysis of the electrochemical performance of the proposed sensor has been provided in Table 1.

Table 1. Comparative performance analysis of ZnO and Pd nanostructured glucose sensors.

Electrode	Method	Sensitivity ($\mu A\ mM^{-1}cm^{-2}$)	LoD (µM)	Linear Range (mM)	Synthesis Time (hrs)	Ref.
ZnO/Co_3O_4/reduced graphene oxide nanocomposite	Amperometric	1551.38	0.043	0.015–10	59	[31]
Pd-Mn alloy nanoparticles supported on reduced graphene oxide	Amperometric	52.16 22.55	1.25	0.0161–1.152 1.152–4.875	49.08	[33]
Nano-ZnO/N-doped porous carbon composites	Amperometric	255.99	0.39	0.002–3.28	29.5	[44]
Cu-doped ZnO nanoparticles	Cyclic Voltammetry	Not provided	0.0007	10^{-6}–0.1	4.5	[45]
CuxO-ZnO composite nanostructures	Amperometric	384.6	0.7	0.03–3	Not provided	[46]
Copper oxide decorated zinc oxide	Amperometric	1142	13.9	1–7	3	[47]
PANI/Pd composite	Cyclic Voltammetry	2140	0.3	0.01–0.1	0.63	[54]
LIG/ZnO/Pd	Amperometric	25.625	130	2–24	0.46	This work

3.5. LIG/ZnO/Pd Sensor Selectivity, Reproducibility, and Shelf Life

The selectivity of the LIG/ZnO/Pd sensor towards glucose detection was evaluated in the presence of commonly encountered interfering species including disaccharides (maltose, sucrose), monosaccharides (fructose), and biologically relevant electroactive species such as dopamine (DA), uric acid (UA), and ascorbic acid (AA). The concentrations of these species are relatively lower than glucose in serum and, therefore, the electrocatalytic oxidation of glucose (2 mM) was investigated in the presence of maltose, fructose, and fructose, UA, DA, and AA (50 µM each). As shown in Figure 6a, the LIG/Pd/ZnO electrode exhibited a distinct and sharp current response upon the addition of 0.2 mM and 2 mM glucose, whereas the subsequent introduction of different sugars (maltose, sucrose, and fructose) yielded negligible changes in the overall current signal. Further addition of UA, DA, and AA (50 µM each) resulted in a slight current change of 0.79, 0.86, and 1.26 µA, respectively, indicating minimal interference. The results indicate the LIG/ZnO/Pd sensor can effectively detect glucose in the presence of interfering analytes and is attributed to the presence of facet-dependent selective electrocatalytic activities of Pd towards glucose oxidation [72,73].

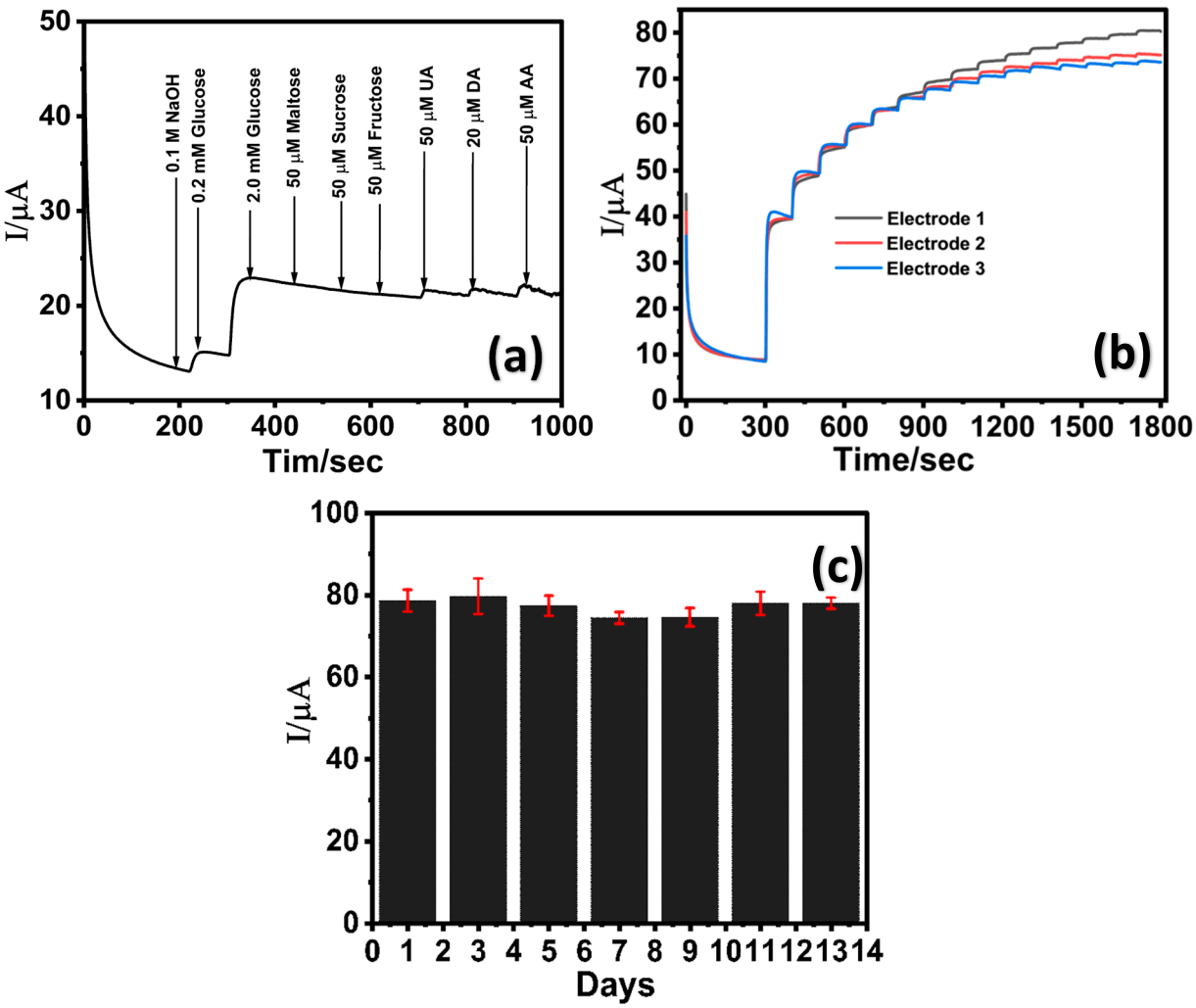


Figure 6. Chronoamperometric response of LIG/ZnO/Pd towards (**a**) 50 μM interfering analytes (maltose, sucrose, fructose, uric acid, dopamine, and ascorbic acid); (**b**) reproducibility analysis via three identically prepared sensors in the presence of varying glucose concentration; (**c**) stability profile of the LIG/ZnO/Pd sensor over a period of 13 days.

The reproducibility of the LIG/ZnO/Pd sensor was assessed by performing chronoamperometric analysis in the presence of varying glucose concentrations at three identically prepared sensors (Figure 6b). A standard deviation of less than 5% was observed from the electrochemical response of three identically prepared sensors, thereby suggesting good reproducibility. The additional reproducibility of three identically fabricated electrodes was assessed across low, medium, and high glucose concentrations (6, 14, 22 mM). As depicted in Table S1 (Supplementary Information), the percent coefficient of variation (% CV) was found to be 0.62, 1.11, and 2.39 (<5%), respectively, suggesting excellent reproducibility attributed to the consistency of the electrode modification process. Further, the LIG/ZnO/Pd exhibited excellent stability over a period of 13 days (Figure 6c) in the presence of 2 mM glucose in 0.1 M NaOH. Although the sensor demonstrates high stability, there was a slight reduction in electrocatalytic activity, retaining ca. 93% of its initial response by the 7th day. These findings highlight that the LIG/ZnO/Pd sensor exhibits good sensitivity, selectivity, reproducibility, and stability towards glucose, thereby suggesting its suitability for non-enzymatic glucose detection.

3.6. Real Sample Analysis

The applicability of the proposed LIG/ZnO/Pd-based glucose sensor was evaluated in artificial urine samples to simulate physiological conditions. To mitigate matrix interference, the samples were diluted 100-fold with 0.1 M NaOH prior to analysis, and known concentrations of glucose (6, 16, 18, and 22 mM) were introduced. Chronoamperometric measurements yielded recovery rates ranging from 88.83% to 102.55%, demonstrating the sensor's capability for accurate glucose quantification in complex biofluids ((Figure S7, Supporting Information) (Table S2, Supporting Information). These results suggest good practical utility and highlight the sensor's robustness and reproducibility under non-ideal sample conditions.

4. Conclusions

In this study, a flexible, scalable, and cost-effective non-enzymatic glucose sensor was successfully developed through the sequential electrodeposition of ZnO and Pd nanostructures onto a porous LIG substrate. The resulting LIG/ZnO/Pd nanostructured electrodes exhibited excellent electrochemical performance, making them highly relevant for detecting elevated glucose levels, especially in diabetic patients. The detailed optimization of the dual-step electrodeposition process significantly contributed to the sensor's broad dynamic detection range (low detection range: 2–10 mM; high detection range: 10–24 mM) with a sensitivity of 25.63 $\mu A \cdot mM^{-1} \cdot cm^{-2}$ and a low LOD of 130 µM. Furthermore, the sensor demonstrated strong anti-interference capabilities, effectively discriminating against glucose from common interferents. In addition to its sensing performance, the proposed sensor offers notable advantages such as flexible substrate, facile fabrication, and excellent reproducibility, underscoring its potential for integration into point-of-care and wearable glucose-monitoring platforms. Future work will explore the incorporation of antifouling strategies, such as Nafion and bovine serum albumin, to mitigate nonspecific adsorption and improve anti-interference capabilities against equimolar concentrations of common interferents such as cysteine, glutathione, lactic acid, lactose, and key electrolytes (Na^+, Ca^{2+}, Cl^-), thereby further enhancing the sensor's selectivity and operational stability in complex biological environments.

Supplementary Materials: The following supporting information can be downloaded at: https://www.mdpi.com/article/10.3390/chemosensors13060201/s1.

Author Contributions: Conceptualization, R.A., A.J. and G.S.; Methodology, R.A. and A.J.; Validation, R.A., A.J. and G.S.; Formal analysis, R.A.; Investigation, R.A. and A.J.; Resources, G.S.; Data curation, R.A.; Writing—original draft, R.A. and A.J.; Writing—review and editing, G.S.; Supervision, G.S.; Project administration, G.S.; Funding acquisition, G.S. All authors have read and agreed to the published version of the manuscript.

Funding: This research received no external funding.

Data Availability Statement: Data is contained within the article or supplementary material.

Conflicts of Interest: The authors declare no conflict of interest.

References

1. Samsu, N. Diabetic Nephropathy: Challenges in Pathogenesis, Diagnosis, and Treatment. *BioMed Res. Int.* **2021**, 1497449. [CrossRef] [PubMed]
2. Indyk, D.; Bronowicka-Szydełko, A.; Gamian, A.; Kuzan, A. Advanced glycation end products and their receptors in serum of patients with type 2 diabetes. *Sci. Rep.* **2021**, *11*, 13264. [CrossRef] [PubMed]
3. Centers for Disease Control and Prevention. National Diabetes Statistics Report. 2024. Available online: https://www.cdc.gov/diabetes/php/data-research/index.html (accessed on 19 April 2025).

4. Parker, E.D.; Lin, J.; Mahoney, T.; Ume, N.; Yang, G.; Gabbay, R.A.; ElSayed, N.A.; Bannuru, R.R. Economic costs of diabetes in the US in 2022. *Diabetes Care* **2024**, *47*, 26–43. [CrossRef] [PubMed]
5. Butt, M.D.; Ong, S.C.; Rafiq, A.; Kalam, M.N.; Sajjad, A.; Abdullah, M.; Malik, T.; Yaseen, F.; Babar, Z.U.D. A systematic review of the economic burden of diabetes mellitus: Contrasting perspectives from high and low middle-income countries. *J. Pharm. Policy Pract.* **2024**, *17*, 2322107. [CrossRef]
6. International Diabetes Federation (IDF). IDF Diabetes Atlas 11th Edition Report 2025. IDF Diabetes Atlas 2025 | Global Diabetes Data & Insights. Available online: https://diabetesatlas.org/resources/idf-diabetes-atlas-2025/ (accessed on 19 April 2025).
7. Nakrani, M.N.; Wineland, R.H.; Anjum, F. *Physiology, Glucose Metabolism*; StatPearls: Tampa/St. Petersburg, FL, USA, 2020. Available online: https://www.ncbi.nlm.nih.gov/books/NBK560599/ (accessed on 19 April 2025).
8. Banday, M.Z.; Sameer, A.S.; Nissar, S. Pathophysiology of diabetes: An overview. *Avicenna J. Med.* **2020**, *10*, 174–188. [CrossRef]
9. Poznyak, A.; Grechko, A.V.; Poggio, P.; Myasoedova, V.A.; Alfieri, V.; Orekhov, A.N. The diabetes mellitus–atherosclerosis connection: The role of lipid and glucose metabolism and chronic inflammation. *Int. J. Mol. Sci.* **2020**, *21*, 1835. [CrossRef]
10. Bolla, A.S.; Priefer, R. Blood glucose monitoring overview of current and future non-invasive devices. *Diabetes Metab. Syndr. Clin. Res. Rev.* **2020**, *14*, 739–751. [CrossRef]
11. Farquhar, A.K.; Henshaw, G.S.; Williams, D.E. Errors in ambient gas concentration measurement caused by the acoustic response of electrochemical gas sensors. *Sens. Actuators A Phys.* **2023**, *354*, 114254. [CrossRef]
12. Teymourian, H.; Barfidokht, A.; Wang, J. Electrochemical glucose sensors in diabetes management: An updated review (2010–2020). *Chem. Soc. Rev.* **2020**, *49*, 7671–7709. [CrossRef]
13. Farquhar, A.K.; Henshaw, G.S.; Williams, D.E. Understanding and correcting unwanted influences on the signal electrode from electrochemical gas sensors. *ACS Sens.* **2021**, *6*, 1295–1304. [CrossRef]
14. Li, Q.; Wu, J.-T.; Liu, Y.; Qi, X.-M.; Jin, H.-G.; Yang, C.; Liu, J.; Li, G.-L.; He, Q.G. Recent advances in black phosphorus-based electrochemical sensors: A review. *Anal. Chim. Acta* **2021**, *1170*, 338480. [CrossRef]
15. Lingbin, O.; Liu, G.; Xia, N. Research progress and application prospects of electrochemical glucose sensors. *Int. J. Electrochem. Sci.* **2021**, *16*, 210633.
16. Mihai, D.A.; Stefan, D.S.; Stegaru, D.; Bernea, G.E.; Vacaroiu, I.A.; Papacocea, T.; Olaru, O.G. Continuous glucose monitoring devices: A brief presentation. *Exp. Ther. Med.* **2022**, *23*, 174. [CrossRef]
17. Jing, Y.; Chang, S.J.; Chen, C.J.; Liu, J.T. Glucose monitoring sensors: History, principle, and challenges. *J. Electrochem. Soc.* **2022**, *169*, 057514. [CrossRef]
18. Thatikayala, D.; Ponnamma, D.; Sadasivuni, K.K.; Cabibihan, J.J.; Al-Ali, A.K.; Malik, R.A.; Min, B. Progress of advanced nanomaterials in nonenzymatic electrochemical sensing and H_2O_2. *Biosensors* **2020**, *10*, 151. [CrossRef] [PubMed]
19. Shen, L.; Liang, Z.; Chen, S.; Wu, C.; Hu, X.; Zhang, J.; Jiang, Q.; Wang, Y. Reusable Electrochemical non-enzymatic glucose sensors based on Au-inlaid nanocages. *Nano Res.* **2022**, *15*, 6490–6499. [CrossRef]
20. Garcia, A.S.M.; Hernandez-Escobar, C.A.; Enriquez-Duran, S.K.; Estrada-Monje, A.; Zaragoza-Contreras, E.A.; Pinon-Balderrama, C.I. Non-Enzymatic Electrochemical Sensing Glucose with Silver Nanoparticles Supported on Poly(3-aminobenzoic acid). *Chemosensors* **2025**, *13*, 133. [CrossRef]
21. Chang, A.S.; Tahira, A.; Solangi, Z.A.; Solangi, A.G.; Ibupoto, M.H.; Chang, F.; Medany, S.S.; Nafady, A.; Kasry, A.; Willander, M.; et al. Pd-Co_3O_4-based nanostructures for the development of enzyme-free glucose sensors. *Bull. Mater. Sci.* **2022**, *45*, 62. [CrossRef]
22. Sakdaphetsiri, K.; Thaweeskulchai, T.; Sukmas, W.; Wang, J.; Schulte, A.; Rodthongkum, N. Laser-Induced Graphene Electrode Modified by Platinum nanoparticle/Zein/Gelatin/Glucose Oxidase for Non-Invasive Glucose Sensor in Multiple Biofluids. *Anal. Chim. Acta* **2025**, *1353*, 343974. [CrossRef]
23. Ayranci, R. The rapid and practical route to Cu@ PCR sensor: Modification of copper nanoparticles upon conducting polymer for a sensitive non-enzymatic glucose sensor. *Electroanalysis* **2021**, *33*, 268–275. [CrossRef]
24. Akter, R.; Saha, P.; Shah, S.S.; Shaikh, M.N.; Aziz, M.A.; Ahammad, A.S. Nanostructured Nickel-based Non-enzymatic Electrochemical Glucose Sensors. *Chem.–Asian J.* **2022**, *17*, e202200897. [CrossRef] [PubMed]
25. Chen, Q.; Chu, D.; Yan, L.; Lai, H.; Chu, X.-Q.; Ge, D.; Chen, X. Enhanced non-enzymatic glucose sensing based on porous ZIF-67 hollow nanoprisms. *New J. Chem.* **2021**, *45*, 10031–10039. [CrossRef]
26. Shruthi Keerthi, D.; Vani, M.M.; Krishnamurthy, B. Green-Synthesized Nanomaterial Coatings for High-Performance Electrodes. *Funct. Coat. Biomed. Energy Environ. Appl.* **2024**, 231–255. [CrossRef]
27. Wu, W.; Miao, F.; Tao, B.; Zang, Y.; Zhu, L.; Shi, C.; Chu, P.K. Hybrid ZnO–graphene electrode with palladium nanoparticles on Ni foam and application to self-powered nonenzymatic glucose sensing. *RSC Adv.* **2019**, *9*, 12134–12145. [CrossRef]
28. Aspoukeh, P.K.; Barzinjy, A.A.; Hamad, S.M. Synthesis, properties and uses of ZnO nanorods: A mini review. *Int. Nano Lett.* **2022**, *12*, 153–168. [CrossRef]
29. Dayakar, T.; Rao, K.V.; Bikshalu, K.; Rajendar, V.; Park, S.-H. Novel synthesis and structural analysis of zinc oxide nanoparticles for the non-enzymatic glucose biosensor. *Mater. Sci. Eng. C* **2017**, *75*, 1472–1479. [CrossRef]

30. Ramírez, D.H.; Romero, G.A.Á.; Huizar, L.H.M.; Galan-Vidal, C.A.; Aguilar-Lira, G.Y. Glucose Determination Using Non-Enzymatic Sensors Based on Fe_2O_3 Nanoparticles. *ECS Trans.* **2022**, *106*, 33. [CrossRef]
31. Hussein, B.A.; Tsegaye, A.A.; Shifera, G.; Taddesse, A.M. A sensitive non-enzymatic electrochemical glucose sensor based on a ZnO/Co_3O_4/reduced graphene oxide nanocomposite. *Sens. Diagn.* **2023**, *2*, 347–360. [CrossRef]
32. Yang, L.; Yang, J.; Dong, Q.; Zhou, F.; Wang, Q.; Wang, Z.; Huang, K.; Yu, H.; Xiong, X. One-step synthesis of CuO nanoparticles based on flame synthesis: As a highly effective non-enzymatic sensor for glucose, hydrogen peroxide and formaldehyde. *J. Electroanal. Chem.* **2021**, *881*, 114965. [CrossRef]
33. Waqas, M.; Lan, J.; Zhang, X.; Fan, Y.; Zhang, P.; Liu, C.; Jiang, Z.; Wang, X.; Zeng, J.; Chen, W. Fabrication of Non-enzymatic Electrochemical Glucose Sensor Based on Pd-Mn Alloy Nanoparticles Supported on Reduced Graphene Oxide. *Electroanalysis* **2020**, *32*, 1226–1236. [CrossRef]
34. Goodnight, L.; Butler, D.; Xia, T.; Ebrahimi, A. Non-Enzymatic Detection of Glucose in Neutral Solution Using PBS-Treated Electrodeposited Copper-Nickel Electrodes. *Biosensors* **2021**, *11*, 409. [CrossRef] [PubMed]
35. Yin, Y.; Zhang, T.; Feng, L.; Ran, J.; Ma, C.; Tan, Y.; Song, W.; Yang, B. Growth of nanostructured Cu_3Al alloy films by magnetron sputtering for non-enzymatic glucose-sensing applications. *RSC Adv.* **2023**, *13*, 14641–14650. [CrossRef] [PubMed]
36. Zhao, T.; Li, W.; Shang, R.; Lei, Y.; Liu, Y.; Ma, C. Experimental and theoretical study on one-step synthesis of AuAg alloy nanoparticle catalytic layer as highly stable non-enzymatic glucose sensing interface. *J. Electroanal. Chem.* **2023**, *950*, 117898. [CrossRef]
37. Lakhdari, D.; Guittoum, A.; Benbrahim, N.; Belgherbi, O.; Berkani, M.; Vasseghian, Y.; Lakhdari, N. A novel non-enzymatic glucose sensor based on NiFe (NPs)–polyaniline hybrid materials. *Food Chem. Toxicol.* **2021**, *151*, 112099. [CrossRef]
38. Gupta, P.; Gupta, V.K.; Huseinov, A.; Rahm, C.E.; Gazica, K.; Alvarez, N.T. Highly sensitive non-enzymatic glucose sensor based on carbon nanotube microelectrode set. *Sens. Actuators B Chem.* **2021**, *348*, 130688. [CrossRef]
39. Dey, B.; Ahmad, W.; Sarkhel, G.; Yang, D.-J.; Choudhury, A. Fabrication of porous nickel (II)-based MOF@ carbon nanofiber hybrid mat for high-performance non-enzymatic glucose sensing. *Mater. Sci. Semicond. Process.* **2022**, *142*, 106500. [CrossRef]
40. González-Sánchez, M.-I.; Khadhraoui, H.; Jiménez-Pérez, R.; Iniesta, J.; Valero, E. non-enzymatic glucose sensor using mesoporous carbon screen-printed electrodes modified with cobalt phthalocyanine by phase inversion. *Microchem. J.* **2024**, *200*, 110314. [CrossRef]
41. Chen, T.; Zhao, P.; Li, J.; Sun, Z.; Huang, W. Construction of a novel Co-based coordination polymer and its study of non-enzymatic glucose sensors. *J. Solid-State Chem.* **2022**, *311*, 123115. [CrossRef]
42. Ariyasajjamongkol, N.; Phasuksom, K.; Paradee, N.; Sirivat, A. Negative current response of non–enzymatic glucose sensor based on pure PEDOT: PSS conductive polymer. *Synth. Met.* **2023**, *297*, 117413. [CrossRef]
43. Raha, S.; Ahmaruzzaman, M. ZnO nanostructured materials and their potential applications: Progress, challenges and perspectives. *Nanoscale Adv.* **2022**, *4*, 1868–1925. [CrossRef]
44. Dai, J.; Huang, J.H.; Gao, L.F.; Qi, Z.K.; Chen, K.F. Green synthesis of Nano-ZnO/N-Doped porous carbon composites for High-Performance Non-Enzymatic electrochemical glucose sensing. *Microchem. J.* **2025**, 113272. [CrossRef]
45. Mahmoud, A.; Echabaane, M.; Omri, K.; Boudon, J.; Saviot, L.; Millot, N.; Chaabane, R.B. Cu-Doped ZnO Nanoparticles for Non-Enzymatic Glucose Sensing. *Molecules* **2021**, *26*, 929. [CrossRef]
46. Manna, A.K.; Guha, P.; Srivastava, S.K.; Varma, S. Non-enzymatic glucose sensors based on electrodeposited Cu_xO–ZnO composite nanostructures. *J. Mater. Sci. Mater. Electron.* **2024**, *35*, 188. [CrossRef]
47. Cheng, C.; Tangsuwanjinda, S.; Cheng, H.; Lee, P. Copper Oxide Decorated Zinc Oxide Nanostructures for the Production of a Non-Enzymatic Glucose Sensor. *Coatings* **2021**, *11*, 936. [CrossRef]
48. Öztürk Doğan, H.; Çepni, E.; Öznülüer Özer, T. Non-enzymatic Amperometric Detection of Glucose on One-Pot Electrochemical Fabricated Pd Nanoparticles-Graphene Modified Electrodes. *Iran. J. Sci.* **2024**, *48*, 389–395. [CrossRef]
49. Liu, Y.-H.; Young, S.-J.; Hsien, C.-Y.; Chu, Y.-L.; Wang, Z.-H.; Chang, S.-J. Improved Non-enzymatic Glucose Sensors of ZnO Nanorods by Adsorb Pt Nanoparticles. *IEEE Trans. Nanotechnol.* **2024**, *23*, 303–310. [CrossRef]
50. Lin, Y.-H.; Sivakumar, C.; Balraj, B.; Murugesan, G.; Nagarajan, S.K.; Ho, M.-S. Ag-Decorated Vertically Aligned ZnO Nanorods for Non-Enzymatic Glucose Sensor Applications. *Nanomaterials* **2023**, *13*, 754. [CrossRef]
51. Vélez, C.A.; Soto-Pérez, J.J.; Corchado-García, J.; Larios, E.; Fulvio, P.F.; Echegoyen, L.; Cabrera, C.R. Glucose oxidation reaction at palladium-carbon nano-onions in alkaline media. *J. Solid-State Electrochem.* **2021**, *25*, 207–217. [CrossRef]
52. Dhara, K.; Mahapatra, D.R. Electrochemical nonenzymatic sensing of glucose using advanced nanomaterials. *Microchim. Acta* **2018**, *185*, 1–32, Erratum in: *Fuel* **2023**, *345*, 128182. [CrossRef]
53. Zhou, J.; Astruc, D. Recent trends and perspectives in palladium nanocatalysis: From nanoparticles to frameworks, atomically precise nanoclusters and single-atom catalysts. *J. Inorg. Organomet. Polym. Mater.* **2024**, *34*, 2903–2925. [CrossRef]
54. Eswaran, M.; Rahimi, S.; Pandit, S.; Chokkiah, B.; Mijakovic, I. A flexible multifunctional electrode based on conducting PANI/Pd composite for non-enzymatic glucose sensor and direct alcohol fuel cell applications. *Fuel* **2023**, *345*, 128182. [CrossRef]

55. Yang, Z.; Yang, H.; Wang, W.; Zhao, H.; Meng, P.; Xie, Y.; Sun, Y. A flexible electrochemical sensor for simultaneous determination of glucose (Glu) and ethanol (Eth) using ZnO and Pd nanoparticles. *J. Appl. Electrochem.* **2023**, *53*, 2013–2023. [CrossRef]
56. Maťátková, O.; Michailidu, J.; Miškovská, A.; Kolouchová, I.; Masák, J.; Čejková, A. Antimicrobial properties and applications of metal nanoparticles biosynthesized by green methods. *Biotechnol. Adv.* **2022**, *58*, 107905. [CrossRef]
57. Thaweeskulchai, T.; Sakdaphetsiri, K.; Schulte, A. Ten years of laser-induced graphene: Impact and future prospects on biomedical, healthcare, and wearable technology. *Microchim. Acta* **2024**, *191*, 292. [CrossRef]
58. Moon, H.-R.; Ryu, B. Review of Laser-Induced Graphene (LIG) Produced on Eco-Friendly Substrates. *Int. J. Precis. Eng. Manuf.-Green. Tech.* **2024**, *11*, 1279–1294. [CrossRef]
59. Sunday, J.; Amoah, K.; Slaughter, G. Growth of electrodeposited ZnO nanowires. *Thin Solid Films* **2015**, *592*, 76–80.
60. El Hafidi, Z.; Outaleb, N.; Naimi, Y. Electrodeposition of ZnO thin films at low temperature: Effects of deposition potential on properties for ZnO/CuO heterojunction solar cells. *J. Mater. Sci. Mater. Electron.* **2024**, *35*, 1861. [CrossRef]
61. Patella, B.; Moukri, N.; Regalbuto, G.; Cipollina, C.; Pace, E.; Di Vincenzo, S.; Aiello, G.; O'Riordan, A.; Inguanta, R. Electrochemical synthesis of zinc oxide nanostructures on flexible substrate and application as an electrochemical immunoglobulin-G immunosensor. *Materials* **2022**, *15*, 713. [CrossRef]
62. Chowdhury, S.R.; Mukherjee, P.; Bhattacharya, S.K. A highly sensitive nonenzymatic glucose sensor based on carbon electrode amplified with PdxCuy catalyst. *Electroanalysis* **2021**, *33*, 820–830. [CrossRef]
63. Thakur, A.K.; Mahbub, H.; Nowrin, F.H.; Malmali, M. Highly robust laser-induced graphene (LIG) ultrafiltration membrane with a stable microporous structure. *ACS Appl. Mater. Interfaces* **2022**, *14*, 46884–46895. [CrossRef]
64. Sarode, A.; Torati, S.R.; Hossain, M.F.; Slaughter, G. A photo-driven bioanode based on MXene-decorated graphene. *Electrochimica Acta* **2024**, *498*, 144637. [CrossRef]
65. Wang, N.; Tao, B.; Miao, F.; Zang, Y. Electrodeposited Pd/graphene/ZnO/nickel foam electrode for the hydrogen evolution reaction. *RSC Adv.* **2019**, *9*, 33814–33822. [CrossRef]
66. Movaghgharnezhad, S.; Kang, P. Laser-induced graphene: Synthesis advances, structural tailoring, enhanced properties, and sensing applications. *J. Mater. Chem. C* **2024**, *12*, 6718–6742. [CrossRef]
67. Thakur, N.; Mehta, D.; Chaturvedi, A.; Mandal, D.; Nagaiah, T.C. Glucose oxidation assisted hydrogen and gluconic/glucaric acid production using NiVP/Pi bifunctional electrocatalyst. *J. Mater. Chem. A* **2023**, *11*, 15868–15877. [CrossRef]
68. Caglar, A.; Düzenli, D.; Onal, I.; Tezsevin, I.; Sahin, O.; Kivrak, H. A novel experimental and density functional theory study on palladium and nitrogen doped few-layer graphene surface towards glucose adsorption and electrooxidation. *J. Phys. Chem. Solids* **2021**, *150*, 109684. [CrossRef]
69. Zhu, Y.; Zhang, X.; Sun, J.; Li, M.; Lin, Y.; Kang, K.; Meng, Y.; Feng, Z.; Wang, J. A non-enzymatic amperometric glucose sensor based on the use of graphene frameworks-promoted ultrafine platinum nanoparticles. *Microchim. Acta* **2019**, *186*, 1–10. [CrossRef]
70. Bi, C.; Lv, H.W.; Peng, H.L.; Li, Q.F. Development of a non-enzymatic glucose electrode based on Au nanoparticles decorated single-walled carbon nanohorns. *J. Mater. Sci. Mater. Electron.* **2021**, *32*, 12705–12715. [CrossRef]
71. Ott, C.E. Strategies for assessing the limit of detection in voltametric methods: Comparison and evaluation of approaches. *Analyst* **2024**, *149*, 4295–4309. [CrossRef]
72. Wang, T.P.; Hong, B.D.; Lin, Y.M.; Lee, C.L. Catalysis of the D-glucose oxidation reaction using octahedral, rhombic dodecahedral, and cubic Pd@Pt core–shell nanoparticles. *Appl. Catal. B Environ.* **2020**, *260*, 118140. [CrossRef]
73. Ye, J.S.; Hsu, S.Y.; Lee, C.L. Sequential and transient electrocatalysis of glucose oxidation reactions by octahedral, rhombic dodecahedral, and cubic palladium nanocrystals. *Electrochim. Acta* **2016**, *211*, 1024–1032. [CrossRef]

Disclaimer/Publisher's Note: The statements, opinions and data contained in all publications are solely those of the individual author(s) and contributor(s) and not of MDPI and/or the editor(s). MDPI and/or the editor(s) disclaim responsibility for any injury to people or property resulting from any ideas, methods, instructions or products referred to in the content.